AIChE WILEY InterScience DISCOVER SOMETHING GREAT

Exploration of Hydrogen Production in a Membrane Reformer

Wei Feng and Tianwei Tan
College of Life Science and Technology, Beijing University of Chemical Technology, Beijing, People's Republic of China

Peijun Ji and Danxing Zheng
College of Chemical Engineering, Beijing University of Chemical Technology, Beijing, People's Republic of China

DOI 10.1002/aic.10797
Published online March 2, 2006 in Wiley InterScience (www.interscience.wiley.com).

Auto-thermal reforming (ATR) is one of the key technologies to produce hydrogen from natural gas. Applying an H_2 membrane to an ATR reactor can simplify the process for pure hydrogen production, and in the meantime can promote methane conversion into hydrogen. Although it is a promising approach and has a great potential application in the future, it is still in an early stage of development. The objective of this work is to systematically study the factors affecting the pure hydrogen production and the thermodynamic efficiency of the integrated process containing an H_2-membrane ATR reactor. The study has been accomplished by the simulation of the H_2-membrane ATR reactor and the thermodynamic analysis of the process. The simulation work is based on the kinetics of the reactions and the mechanisms of membrane permeation. The effects of factors including the flowing mode of sweeping gas, the rate of sweeping gas, the inlet rate of CH_4, and the inlet ratio of CH_4 to H_2O, on the production rate of separated H_2, on the driving force of hydrogen permeation, and on the thermodynamic efficiency of the integrated process have been explored. The results will have a significant contribution to the design of an H_2-membrane ATR reactor and an integrated process for pure hydrogen production. *AIChE J,* 52: 2260–2270, 2006
Keywords: reactor simulation, H_2-membrane reactor, thermodynamic efficiency, auto-thermal reforming

Introduction

Hydrogen is generally regarded as an important future energy carrier with a fuel cell as its converter. Although H_2 can be produced from a wide variety of resources using a range of different technologies, natural gas is generally preferred and will remain in the near future the major feedstock for the manufacture of H_2.[1, 2] Auto-thermal reforming (ATR) is one of the key technologies for hydrogen production from natural gas.[3,4] With air, methane, and steam as the feed, in an auto-thermal reformer, part of the methane is oxidized to provide heat, and the other part of methane is reformed to produce syngas on an Ni catalyst.[5] The produced synthesis gas is a mixture of H_2, CO, CO_2, steam, N_2(from the air), and unconverted CH_4. Because CO can damage a polymer electrolyte membrane fuel cell, generally, two water-gas-shift reactors and a selective oxidization reactor are employed in order to control the concentration of CO.[6] For the synthesis gas, the fuel cell does not convert some 25% of H_2 that is fed into it.[7,8] If H_2 is separated from the synthesis gas, the problems can be avoided. One of the solutions is the use of an H_2-membrane reactor, which can combine a separator and a reactor in one process step. Recently, many investigators have studied different types of reactors applied with H_2 membrane to produce hydrogen,

Correspondence concerning this article should be addressed to P. Ji at Jipj@mail.buct.edu.cn.

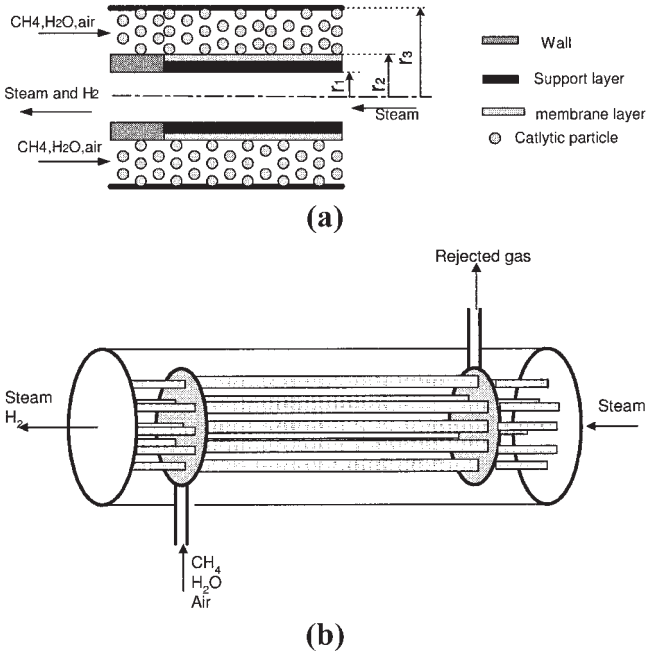

Figure 1. (a) H_2-membrane ATR reactor; (b) the layout of multiple membrane tubes.

and they have found that the thermodynamic equilibrium limitation associated with reversibility of the reactions can be "broken" using an H_2 permeable membrane.[9-11]

In this work, an H_2-membrane ATR reactor was studied, which consists of 100 membrane tubes. The schematic of the configuration of a membrane tube and the conceptual layout of multiple reactor tubes are shown in Figures 1a and 1b, respectively. In an H_2-membrane tube, methane, water, and air are fed into the shell side as reactants, and in the non-reaction side, steam is flowed in as the sweeping gas to promote the permeation of H_2 through the H_2-permeable membrane. The sweeping gas can flow through the H_2-membrane ATR reactor either in a co-current mode or in a counter-current mode.

The integrated process around the H_2-membrane ATR reactor is shown in Figure 2, which consists of an H_2-membrane ATR reactor, a heat exchanger, a catalytic burner, and compressors as the main units. Through the heat exchanger, the heat carried by the stream of H_2 and water from the reactor is recovered to generate steam as the sweeping gas. Through the catalytic burner, the heat of the stream of rejected gas from the reactor is recovered to heat up the reactants and to generate steam as the sweeping gas. If more heat is required, extra CH_4 is needed. The aim of this work is to systematically study the factors affecting pure hydrogen production, the driving force of hydrogen permeation, and the thermodynamic efficiency of the integrated process through rigorous simulation based on the kinetics of the reactions and the mechanisms of membrane permeation.

Simulation

H_2-membrane auto-thermal reforming (ATR) reactor

For the simulation of an H_2-membrane ATR reactor provided with Ni-Al_2O_3 catalyst, a one-dimensional steady-state heterogeneous model is adopted. Plug flow at both sides of the membrane has been assumed. The influence of intra-particle concentration gradients within the catalyst pellet is taken into account by solving the solid phase continuity equation at each increment along the adiabatic fixed bed reactor's axial coordinate. The gas-phase continuity, energy, and solid continuity equations in the reaction side, as well as the continuity and energy equations in the non-reaction side, are presented in Table 1, in which the corresponding inlet and boundary conditions are also listed. The energy equations in Table 1 take into account the heat of reaction, the heat exchanged between the non-reaction zone and the reaction zone, and the heat carried by the diffusion of hydrogen. Since the pressure drop has been shown negligible,[10,12] the pressure drop along the reactor's axial coordinator is not considered.

The simulation of an H_2-membrane ATR reactor is based on the kinetics of the methane combustion reaction, the kinetics of steam reforming to CO and CO_2, and the kinetics of the water-gas shift reaction.[13,14] The influence of carbon deposition and that of the cracking of methane on the catalyst activity were neglected. The rate equations, as well as the kinetic parameters applied in the calculations of the reaction rate, are summarized in Tables 2, 3, and 4. In the reaction side, the subscript i represents gas species, that is, CH_4, H_2O, CO, H_2, CO_2, O_2, and N_2. In the solid-phase continuity equation, the effective diffusivity of component i is related to the molecular and Knudsen diffusivities. The effective diffusivities are calculated according to the method in the literature[15]. The physical chemical properties Cp_i,[16] equilibrium constants,[17] and diffusivities[18] are considered to be a function of temperature. For a multi-component mixture, molecular diffusion is generally described by the Stephan-Maxwell approach. However, minor differences in calculated concentration profiles were observed between the Stephan-Maxwell approach and the binary diffusion approach.[5] Due to the small differences in diffusion coefficient of the different products and reactants, in this work, the diffusion in the catalyst particle is described by Fick's law.

The permeability of hydrogen through the H_2-permeable membrane is calculated according to Eq. 1:

$$N_{H_2} = \frac{P_m \exp\left(-\frac{E_A}{R\bar{T}}\right)}{\delta_{H_2}} \left(\sqrt{p_{H_2}^{high}} - \sqrt{p_{H_2}^{low}}\right) \quad (1)$$

The apparent activation energy E_A and pre-exponential factor P_m of the membrane are 29.73 kJ/mol and 7.71×10^{-4} mol m/(s m^2 $bar^{0.5}$), respectively.[10]

The characteristic parameters used for describing the H_2-membrane ATR reactor are listed in Table 5. The H_2 membrane is applied from 0.2 meters away from the inlet of the reactor because the temperature at the beginning of the reactor is too high and not suitable for the operation of an H_2 membrane.

The H_2 membrane consists of two layers (see Figure 3), a support layer with large pores and a dense membrane layer. The thickness of the support layer (δ_{sp}) is assumed to be 0.005m. To simulate as closely as possible by means of the one-dimensional models, the cross-sectional averaged temperatures of the reaction region and the non-reaction region are calculated by using an averaged thermal conductivity k_m, with which the effect of heat transfer through the packed bed has been taken into consideration. The averaged thermal conductivity k_m is calculated with Eq. 2:

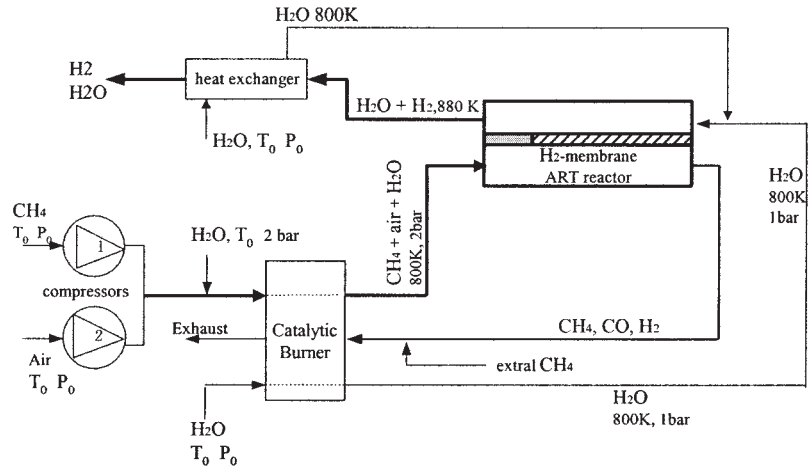

Figure 2. Integrated process with an H_2-membrane ATR reactor of constrained geometry for pure H_2 production.

$$\frac{1}{k_m} = \frac{1}{k_{SP}} + \frac{r_3 - r_2}{\delta_{SP} k_s} \tag{2}$$

where $r_3 - r_2$ represents the "thickness" of the catalyst bed. k_{sp} and δ_{sp} are the thermal conductivity and thickness of the support layer, respectively. The thermal conductivity k_s of the porous catalyst Ni-Al_2O_3 is about 0.3J/(m s K).[19] Since the thermal conductivity of the support layer, such as ceramic Al_2O_3, is about 8 J/(m s K) at around 1000K [20], which is much larger than that of the catalyst bed, the heat transfer resistance mainly comes from the packed bed. According to the data mentioned above, the averaged thermal conductivity k_m is about 0.15J/(m s K).

The solid-phase continuity equation in Table 1 is solved by difference methods. The number of collocation points defined depends on the effect on the final calculation results. Normally, 10 collocation points are defined. The resulting difference equations are solved at each increment of the reactor's axial coordinate. In each reactor increment, the intra-particle concentration gradients of the previous step are used as the initial value of the next step to solve the solid-phase continuity equations; thus, rapid convergence is obtained. The effectiveness factors and the molar fractions of different species as a function of the reactor's axial coordinate are shown in Figures 4a and 4b. As shown in Figure 4a, the effectiveness factors change slightly along the reactor's axial coordinate. Figure 4b shows the axial profiles of the molar fraction of the different species in the H_2-membrane ATR reactor. Because of the continuous removal of H_2 from the reaction zone, the reforming and water-gas-shift reactions are driven towards more H_2 formation; thus, the molar fraction of CO_2 is much higher than CO at the end of the reactor.

Compressor

The electric power used in the compressor is calculated by Eq. 3,[21] assuming compressor exergy efficiency η_{cp} of 50%.

$$W_{cp} = \frac{F_t R T_0}{\eta_{cp}} \ln \frac{P_{in}}{P_0} \tag{3}$$

Catalytic burner

A catalytic burner is used to heat the reactants and part of the sweeping gas to the inlet temperature. The remaining H_2, CO, CO_2, N_2, H_2O, and CH_4 in the rejected gas of the membrane reactor are introduced into the furnace. If the remaining H_2, CO, and CH_4 in the rejected gas of the H_2-membrane ATR reactor are not enough to provide the heat required, extra CH_4 is introduced into the furnace in order to satisfy the heating requirement. The temperature of the after-combustion gas mixture leaving the furnace is set to be 353K. The amount of extra CH_4 input into the furnace $F_{Extra\ CH_4}$ is calculated by Eq. 4:

$$F_{Extra\ CH_4} = \left(\frac{\Delta H_{heating}}{\eta_{Burner}} + \Delta H\big|_{T_{fg}}^{T_0} + \Delta H\big|_{T_0}^{353} + \sum_{l}^{3} F_l \Delta H_l^{com} \right) / \Delta H_{CH_4}^{com} \tag{4}$$

in which $\Delta H_{heating}$ is the heat required for heating the reactants and part of the steam (as sweeping gas) up to the inlet temperature T_{in} (800 K) of the ATR reactor. η_{Burner} represents the efficiency of the catalytic burner. F_l and ΔH_l^{com} represent molar flow rate and the combustion heat at T_0 of component l, respectively. Subscript l represents the remaining CH_4, CO, and H_2 in the rejected gas. $\Delta H\big|_{T_0}^{353K}$ is the heat required by all the after combustion species (CO_2, H_2O, and N_2) to elevate the temperature from T_0 to 353K (the outlet temperature of the catalytic burner). $\Delta H\big|_{T_{fg}}^{T_0}$ is the heat that is released by cooling the rejected gas from T_{fg} (the outlet temperature of rejected gas from the H_2-membrane ATR reactor) to T_0. In this work, 20% of heat loss in the furnace and heat exchangers is assumed.

Process efficiency

The product of the integrated process shown in Figure 2 is pure H_2. The thermodynamic efficiency η_{Ex} is an important parameter for a process.[22,23] In this work, it is defined as the exergy of the separated H_2 over the total exergy input, as shown in Eq. 5:

Table 1. The Models for the H_2-Membrane ATR Reactor

Reaction side

Gas phase continuity equation

$$\frac{dF_i}{dz} = a_r(1-\varepsilon_B)\rho_s^{ART}\sum_{k=1}^{N_R}(\eta_k \upsilon_{ik} R_k) - a_{H_2} N_i^{H_2}$$

$$N_4^{H_2} = N_{H_2};\ N_i^{H_2} = 0,\ i \neq 4$$

Gas phase energy equation

$$\frac{dT_r^{ART}}{dz} = \frac{1}{\sum_{i=1}^{6} F_i C_{P_i}} \times \left[a_r \rho_s^{ART}(1-\varepsilon_B)\sum_{k=1}^{N_R}(-\Delta H_k \eta_k R_K) - q - a_{H_2} N_{H_2} \Delta H_{H_2} \right]$$

$$q = \frac{a_{H_2} k_m}{\delta_{sp}}(T_r^{ART} - T_{nrH_2}^{ART})$$

Solid phase equations for calculating the effectiveness factors

$$\frac{1}{\xi^2}\frac{d}{d\xi}\left(D_{e,i}\xi^2 \frac{dp_{s,i}}{d\xi}\right) = 10^{-5} RT \rho_s^{ART} r_s^2 \sum_{k=1}^{N_R}(\nu_{i,k} R_{s,k})$$

$$a_\nu \frac{D_{e,i}}{r_s}\frac{dp_{s,i}}{d\xi}\bigg|_{\xi=1} = 10^{-5} RT \sum_{k}^{N_B}(\eta_k \upsilon_{ik} R_k)$$

Solid phase boundary conditions

$$\xi = 0,\ \frac{dp_{s,i}}{d\xi} = 0$$

Gas phase boundary conditions

$$z = 0,\ F_i = F_i|_{z=0},\ T = T_{in}$$

Non-reaction side

Continuity equation

$$\frac{dG_{H_2}}{dz} = a_{H_2} N_{H_2}$$

Energy equation

$$\frac{dT_{nrH_2}^{ART}}{dz} = \frac{1}{\sum_j G_j C_{p_j}}[q + a_{H_2} N_{H_2} \Delta H_{H_2}]$$

$$\eta_{Ex} = \frac{Ex_{H_2}^S}{Ex_{input1} + Ex_{input2} + W_{CP}} \quad (5)$$

Ex_{input1} represents the exergy of the reactants and the sweeping gas at T_0 and P_0. The exergy of extra CH_4 input into the furnace is represented by Ex_{input2}.

Simulation Results

Effect of flowing modes of sweeping gas

For the H_2-membrane ATR reactor, the sweeping gas of steam can be introduced into the permeate side of the reactor either in a counter-current mode or in a co-current mode. The simulation of the H_2-membrane reactor with a co-current mode has been described above. The H_2-membrane reactor with a counter-current mode can also be simulated by a step-wise numerical procedure. It begins with a fixed production rate of separated H_2 for a hypothetical flowing rate of sweeping gas at $z = 0$ on the permeate side. An outlet temperature of separated H_2 has to be assumed. The convergence (the molar rate of separated H_2 is zero at the end of the reactor) is achieved by repeating the calculation.

Table 3. Parameter Values for the Expression $k_k = k_k^0 \exp(-E_{a,k}/RT)$

Reaction	k_k^0 $[mol/(kg_{cal} \cdot s)]$	$E_{a,k}$ $[J/mol]$
1. $k_{1,a}$, $k_{1,b}$	3.14×10^{-4}, 2.64×10^{-4}	—
2. k_2	1.17×10^{15} bar$^{0.5}$	240.1×10^3
3. k_3	5.43×10^5 bar^{-1}	67.13×10^3
4. k_4	2.83×10^{14} bar$^{0.5}$	243.9×10^3

As described in Eq. 1, the permeability of an H_2 membrane increases with the working temperature of the membrane and the difference in the square root of partial pressure of the hydrogen across the membrane, $\sqrt{p_{H_2}^{high}} - \sqrt{p_{H_2}^{low}}$. Figure 5 shows the temperature profiles of the reaction side and the permeate side, when the sweeping gas flows at the same inlet rate in a co-current mode and in a counter-current mode, respectively. The average temperature in a counter-current mode is a bit lower than that in a co-current mode from z 0.2 until the end of the reactor. Figure 6 presents the effect of the flowing mode on $\sqrt{p_{H_2}^{high}} - \sqrt{p_{H_2}^{low}}$, which is defined as the driving force of the hydrogen permeation. From z 0.2, the driving force of hydrogen permeation in a co-current mode decreases along the reactor length, whereas the counter-current mode has a relatively flat driving force along the reactor length. The average driving force of the counter-current mode is larger than that of the co-current mode. Although the operating temperature of the membrane is a bit lower in a counter-current mode than in a co-current mode, due to a larger average driving force for hydrogen permeation, for a given inlet rate of sweeping gas, the H_2-membrane ATR reactor in a counter-current mode separates more hydrogen than it does in a co-current mode, as shown in Figure 7.

For getting the same production rate of hydrogen separated, the counter-current mode needs less steam as the sweeping gas, for example, 3.6 mol/s in a counter-current mode compared to 10.0 mol/s in co-current mode, as presented in Figure 8.

Table 2. Reaction Rate for the Reactions in the H_2-Membrane ATR Reactor

Reactions	Kinetics of Reaction
1. $CH_4 + 2O_2 \Leftrightarrow 2CO_2 + 2H_2O$	$R_1 = \frac{k_{1,a} x_{CH_4} x_{O_2}}{(1 + K_{CH_4}^0 x_{CH_4} + K_{O_2}^0 x_{O_2})^2} + \frac{k_{1,b} x_{CH_4} x_{O_2}^{1/2}}{(1 + K_{CH_4}^0 x_{CH_4} + K_{O_2}^0 x_{O_2})}$
2. $CH_4 + H_2O \Leftrightarrow CO + 3H_2$	$R_2 = \frac{(k_2/p_{H_2}^{2.5})(p_{CH_4} p_{H_2O} - p_{H_2}^3 p_{CO}/K_{eq2})}{DEN^2}$
3. $CO + H_2O \Leftrightarrow CO_2 + H_2$	$R_3 = \frac{(k_3/p_{H_2})(p_{CO} p_{H_2O} - p_{H_2} p_{CO_2}/K_{eq3})}{DEN^2}$
4. $CH_4 + 2H_2O \Leftrightarrow CO_2 + 4H_2$	$R_4 = \frac{(k_4/p_{H_2}^{3.5})(p_{CH_4} p_{H_2O}^2 - p_{H_2}^4 p_{CO_2}/K_{eq4})}{DEN^2}$

Note: $DEN = 1 + K_{CO} p_{CO} + K_{H_2} p_{H_2} + K_{CH_4} p_{CH_4} + K_{H_2O} p_{H_2O}/p_{H_2}$

Table 4. Parameter Values for the Expression $K_i = K_i^0 \exp(-\Delta H_{ads,i}/RT)$

Adsorption Coefficient	K_i^0	$\Delta H_{ads,i}$ [kJ/mol]
$K^0_{CH_4}$	6.67×10^{-2}	—
$K^0_{O_2}$	4.34×10^{-5}	—
K_{CH_4}	6.65×10^{-4} bar^{-1}	−38.28
K_{CO}	8.23×10^{-5} bar^{-1}	−70.65
K_{H_2}	6.12×10^{-9} bar^{-1}	−82.90
K_{H_2O}	1.77×10^{5}	88.68

The above results indicate that the counter-current mode has advantages over the co-current mode. So, in the following sections, the counter-current mode is chosen as the flowing mode of the sweeping gas.

Effect of the inlet rate of CH_4 to the reactor

Figure 9 shows the axial temperature profiles of the reaction side and the permeate side of the H_2-membrane ATR reactor at different inlet rates of CH_4 to the reactor. The average temperature of the reaction side and the permeate side of the inlet rate of CH_4 at 1.4 mol/s is higher than that of the inlet rate of CH_4 at 0.8 mol/s. From z 0.2 until the end of the reactor, in the reaction side, the molar flow rate of H_2 for the inlet rate of CH_4 at 1.4 mol/s is higher than that of the inlet rate of CH_4 at 0.8 mol/s, as shown in Figure 10. Because there is more H_2 in the reaction side, the average driving force of H_2 permeation at the inlet rate of CH_4 of 1.4 mol/s is larger than that at the inlet rate of CH_4 of 0.8 mol/s, as illustrated in Figure 11. Due to the higher average temperature and the larger driving force of H_2 permeation, the production rate of separated H_2 increases with the inlet rate of CH_4 to the reactor; see Figure 12.

However, the fraction of hydrogen recovered (defined as the ratio of separated H_2 to the total useful products of CO and H_2) and the CH_4 conversion decrease as the inlet rate of CH_4 to the reactor increases, as illustrated in Figures 13 and 14, respectively. As the inlet rate of CH_4 to the reactor increases, because of the lower fraction of hydrogen recovered and the lower CH_4 conversion, the amount of remaining fuel in the rejected gas from the reactor increases, and the extra methane input into the furnace decreases.

The relationship between the production rate of separated H_2 per overall CH_4 (including the CH_4 to the reactor and the extra CH_4 fed into the furnace) and the inlet rate of CH_4 to the reactor is shown in Figure 15. For the sweeping gas at 10 mol/s, the production rate of separated H_2 per overall CH_4 gets the highest value when the inlet rate of CH_4 to the reactor is at 0.95 mol/s.

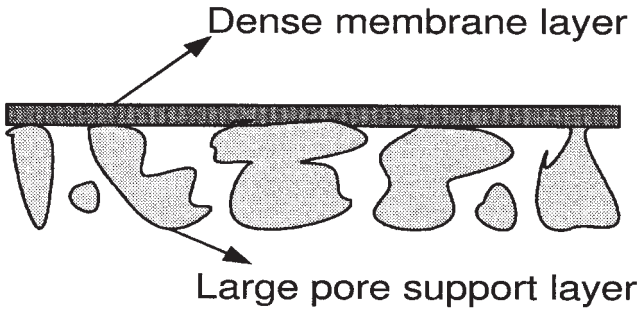

Figure 3. H_2-membrane configuration.

The above results can be reflected in the thermodynamic efficiency of the process. As shown in Figure 16, for the sweeping gas at 10 mol/s, the thermodynamic efficiency peaks at the inlet rate of CH_4 to the reactor of 0.95 mol/s. From the results shown in Figures 15 and 16, the inlet rate of CH_4 to the reactor of 0.95 mol/s is suggested as the appropriate one for the sweeping gas at 10 mol/s.

Effect of the inlet ratio CH_4/H_2O to the reactor

More steam in the feed promotes the water-gas-shift reaction, so the H_2 molar flow rate in the gas mixture with an inlet ratio of CH_4/H_2O of 1/4 is higher than that with the ratio of 1/1.5 from z 0.23 m, as shown in Figure 17. However, more inlet steam leads to a lower partial pressure of the H_2 in the reaction side, so the average driving force of hydrogen permeation at a higher inlet ratio of CH_4 to steam is larger than that at a lower inlet ratio of CH_4 to steam, where the H_2 membrane is applied (z 0.2m), as shown in Figure 18. The effect of inlet ratio CH_4/H_2O to the reactor on the axial temperature profiles of the reaction side and the permeate side are indicated in Figure 19. There is no significant difference in the average temperature of the reaction side and the permeate side for different inlet ratio CH_4/H_2O from z 0.2 m.

Mainly due to the increasing of the driving force of hydrogen permeation, the production rate of separated H_2 increases with the inlet ratio CH_4/H_2O, as shown in Figure 20. The same trend can be observed for the overall exergy efficiency of the pro-

Table 5. Parameters for Describing the H_2-Membrane ATR Reactor

Tube inside radius r_1 [m]	0.01
Tube outside radius r_2 [m]	0.015
Inner radius of the shell r_3 [m]	0.025
Reactor length L [m]	0.65
Inlet temperature of reactants and sweeping gas [K]	800
Inlet pressure at shell side |	2
Inlet pressure at tube side |	1
Membrane thickness δ [μm]	5
Averaged thermal conductivity of membrane tube k_m [$J \cdot m^{-1} \cdot s^{-1} \cdot K^{-1}$]	0.15
Number of membrane tubes n_{tube}	100
Catalyst capacity	
Void fraction of packing ε_b	0.43
Radius of catalyst particle for membrane ATR r_s [m]	2.5×10^{-3}
Catalyst density ρ_s [$kg \cdot m^{-3}$]	2100

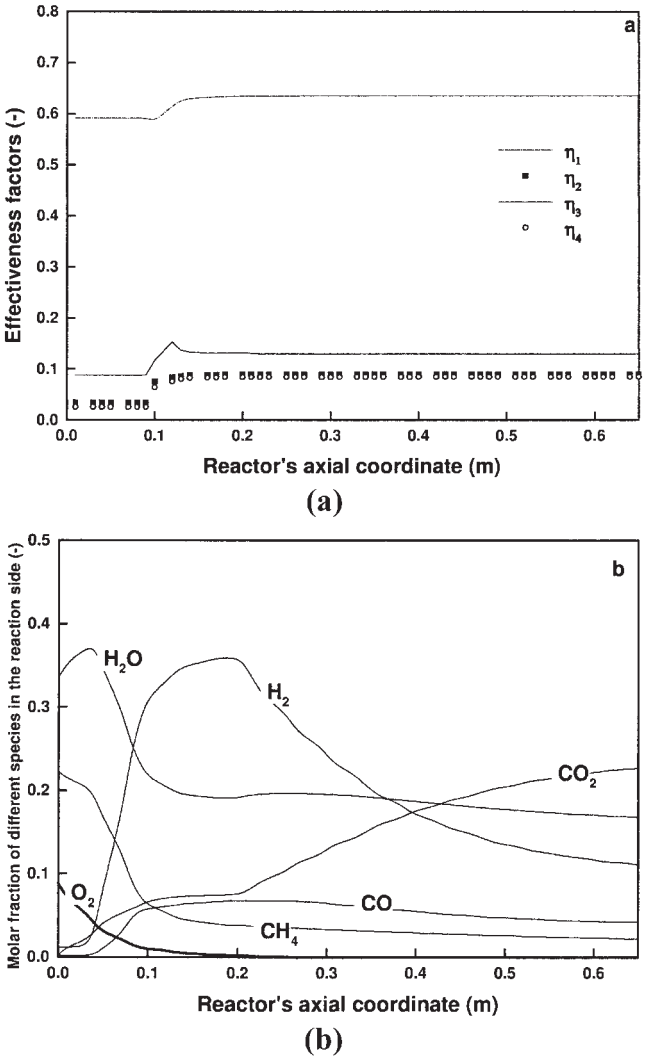

Figure 4. (a)The effectiveness factors vs. the reactor's axial coordinate; (b) the molar fractions of different species vs. the reactor's axial coordinate.

The sweeping gas flows in a co-current mode. The inlet rate of CH_4 to the reactor is 0.95 mol/s. The inlet ratio $CH_4/H_2O/O_2$ = 1/1.5/0.4.

cess; the process gets a higher thermodynamic efficiency at a higher inlet ratio CH_4/H_2O—see Figure 21. However, it is not necessary to increase the ratio CH_4/H_2O higher than 1/1.5, as the production rate of separated H_2 and the thermodynamic efficiency increased little after that.

Effect of the sweeping gas

Figures 22, 23, and 24 illustrate the production rate of separated H_2, the fraction of H_2 recovered, and CH_4 conversion as a function of the inlet rate of CH_4 to the reactor, respectively. A higher rate of sweeping gas can promote more CH_4 converted and more H_2 recovered, resulting in a higher production rate of separated H_2.

However, the above results do not mean that the increasing of the rate of sweeping gas is always necessary. For a certain

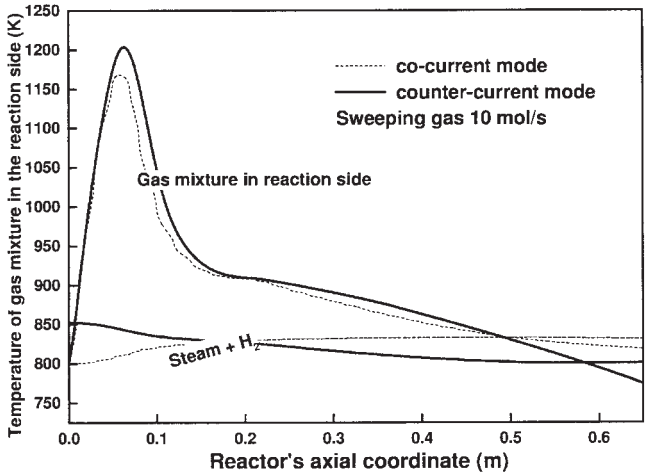

Figure 5. The reactor's temperature profiles of the gas mixture in the reaction side and permeate side, when the sweeping gas flows in a co-current mode and in a counter-current mode, respectively.

The inlet rate of CH_4 to the reactor is 0.95 mol/s. The inlet ratio $CH_4/H_2O/O_2$ = 1/1.5/0.4.

inlet rate of CH_4, there is a rate of sweeping gas that is just sufficient to separate the produced hydrogen maximally; further increase of the rate of sweeping gas will result in a negligible increase in the production rate of H_2 separated. This rate is defined as the appropriate rate of sweeping gas. For different inlet rates of CH_4, the appropriate rates of sweeping gas have been found as shown in Figure 25. Correspondingly, Figure 26 shows the production rates of separated H_2 at the appropriate rates of sweeping gas for different inlet rates of CH_4.

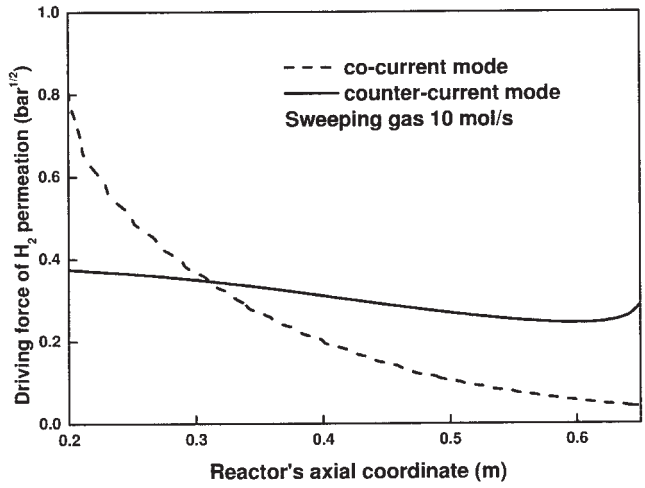

Figure 6. The driving force of H_2 permeation along the reactor's axial coordinate, when the sweeping gas flows in a co-current mode and in a counter-current mode, respectively.

The inlet rate of CH_4 to the reactor is 0.95 mol/s. The inlet ratio $CH_4/H_2O/O_2$ = 1/1.5/0.4.

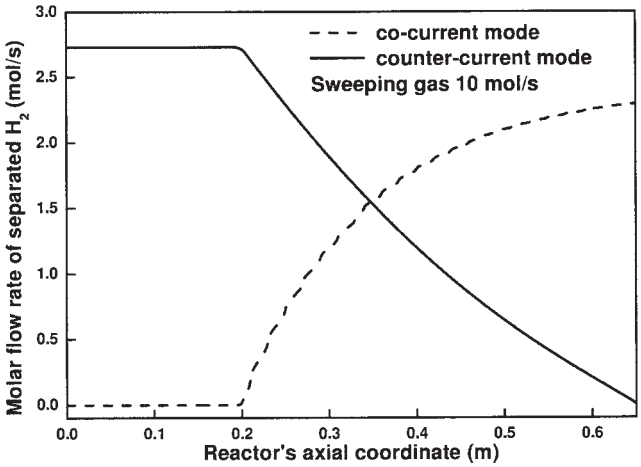

Figure 7. The molar flow rate of separated H_2 along the reactor's axial coordinate, when the sweeping gas flows in a co-current mode and in a counter-current mode, respectively.

The inlet rate of CH_4 to the reactor is 0.95 mol/s. The inlet ratio $CH_4/H_2O/O_2$ = 1/1.5/0.4.

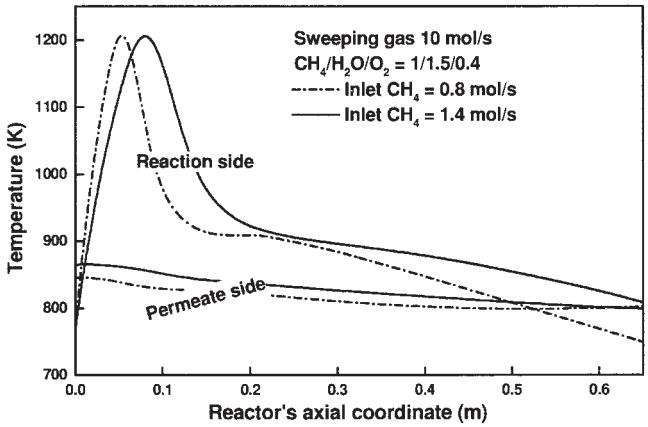

Figure 9. The temperature profile of the gas mixture for different inlet rates of CH_4 to the reactor.

The sweeping gas flows at 10 mol/s in a counter-current mode.

Conclusions

For the H_2-membrane ATR reactor with constrained geometry and the relevant process for pure hydrogen production, based on rigorous simulations, the factors affecting the production rate of separated H_2 and the thermodynamic efficiency have been studied systematically.

To get the same production rate of separated H_2, the H_2-membrane reactor requires less sweeping gas flowing in a counter-current mode. If the same rate of sweeping gas is used, the H_2 membrane can separate more H_2 in a counter-current mode than in a co-current mode. So, the counter-current mode is suggested as the flowing mode of the sweeping gas.

By considering the effect of the inlet rate of CH_4 on the production rate of separated H_2, on the fraction of H_2 recovered, on the methane conversion, on the production rate of separated H_2 per overall CH_4, and on the thermodynamic efficiency, an appropriate inlet rate of CH_4 can be found. The production rate of separated H_2 per overall CH_4 and the thermodynamic efficiency of the process peak at the appropriate inlet rate of CH_4.

The production rate of separated H_2 and thermodynamic efficiency increase with the increase of the inlet ratio CH_4/H_2O. However, it is not necessary to increase the ratio CH_4/H_2O higher than 1/1.5, as the production rate of separated H_2 and the thermodynamic efficiency increased little after that.

By considering the effect of the rate of sweeping gas on the production rate of separated H_2, on the fraction of H_2 recovered, and on the CH_4 conversion, corresponding to an inlet rate of CH_4, the appropriate rate of sweeping gas can be

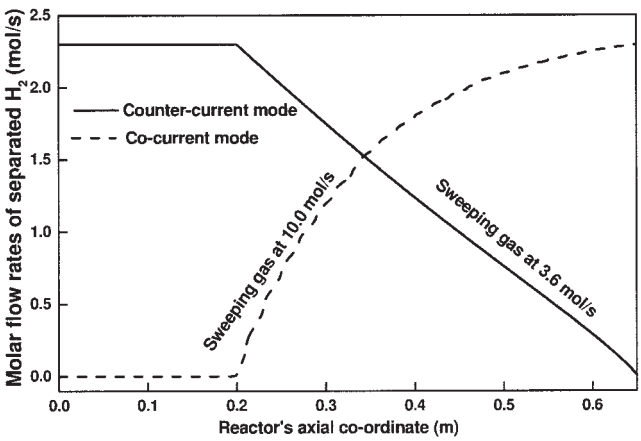

Figure 8. Molar flow rate of separated H_2 along the reactor's axial coordinate.

The molar flow rates of sweeping gas are 10 mol/s in a co-current mode and 3.6 mol/s in a counter-current mode, respectively. The inlet rate of CH_4 to the reactor is 0.95 mol/s. The inlet ratio $CH_4/H_2O/O_2$ = 1/1.5/0.4.

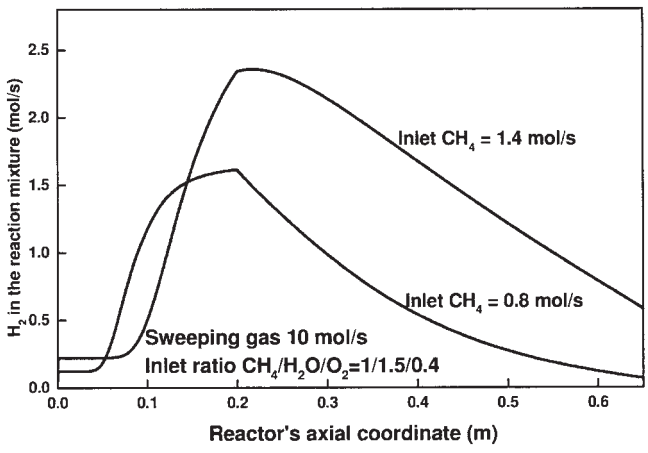

Figure 10. The molar flow rate of H_2 in the reaction side of the H_2-membrane reactor along the reactor's axial coordinate at different inlet rates of CH_4 to the reactor.

The sweeping gas flows at 10 mol/s in a counter-current mode.

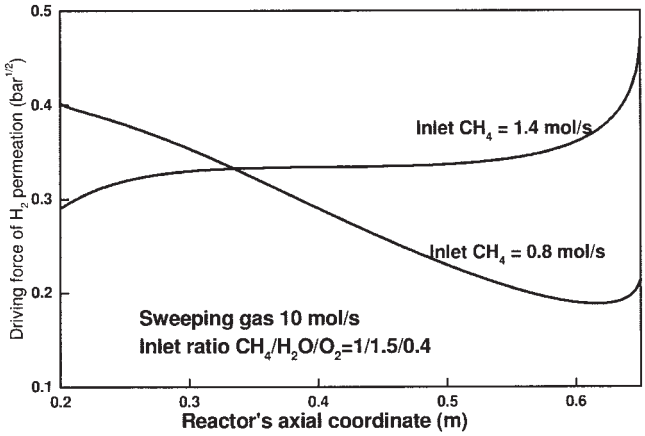

Figure 11. The driving force of H_2 permeation along the reactor's axial coordinate at different inlet rates of CH_4 to the reactor.

The sweeping gas flows at 10mol/s in a counter-current mode.

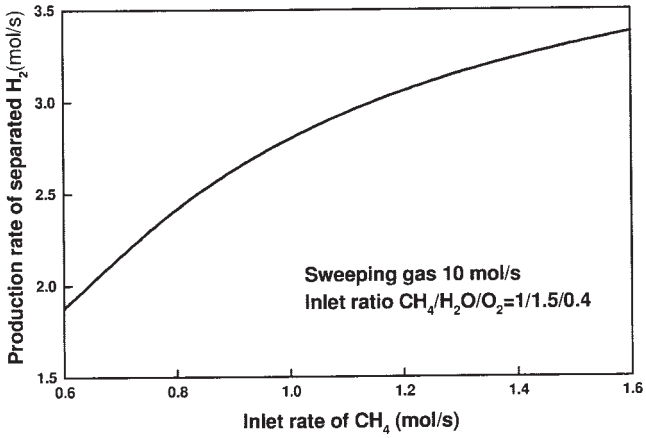

Figure 12. The production rate of separated H_2 vs. the inlet rate of CH_4 to the reactor.

The sweeping gas flows at 10 mol/s in a counter-current mode.

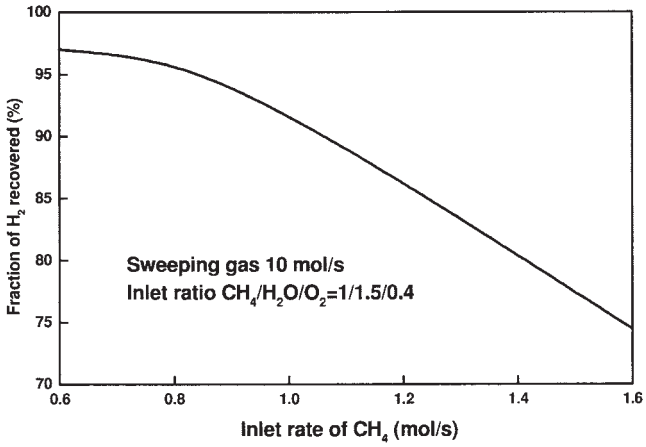

Figure 13. The fraction of H_2 recovered vs. the inlet rate of CH_4 to the reactor.

The sweeping gas flows at 10 mol/s in a counter-current mode.

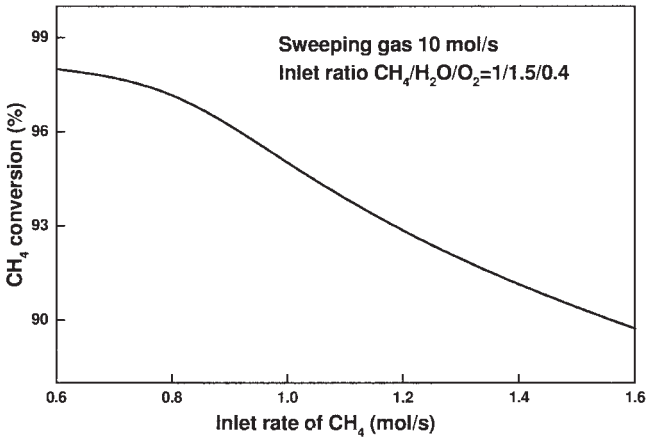

Figure 14. The CH_4 conversion at different inlet rates of CH_4 to the reactor.

The sweeping gas flows at 10 mol/s in a counter-current mode.

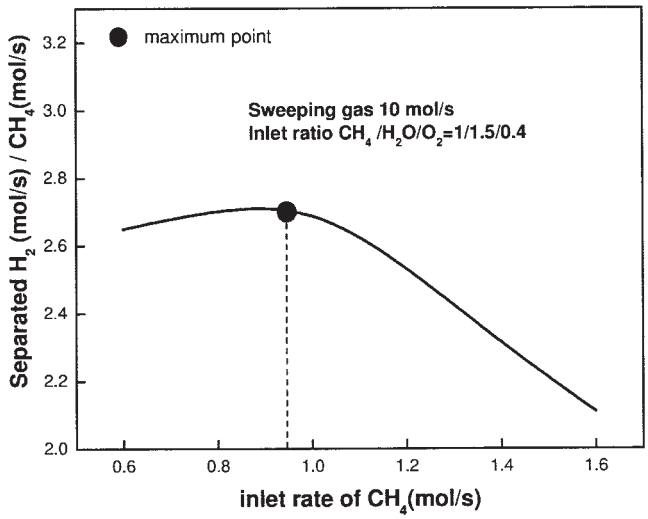

Figure 15. Production rate of separated H_2 per overall CH_4 vs. the inlet rate of CH_4 to the reactor.

The sweeping gas flows at 10 mol/s in a counter-current mode.

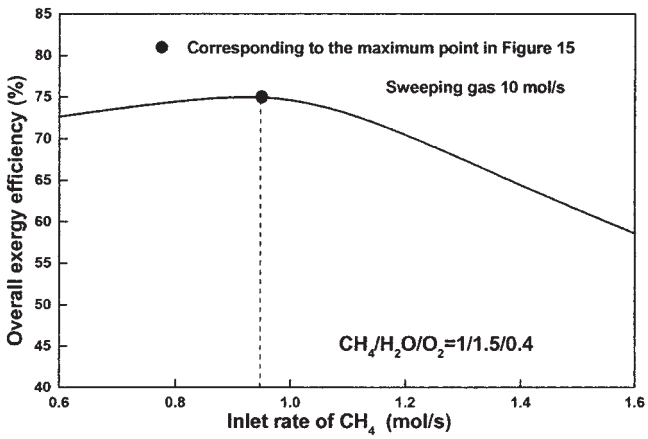

Figure 16. The overall exergy efficiency of the integrated process vs. the inlet rate of CH_4 to the reactor.

The sweeping gas flows at 10 mol/s in a counter-current mode.

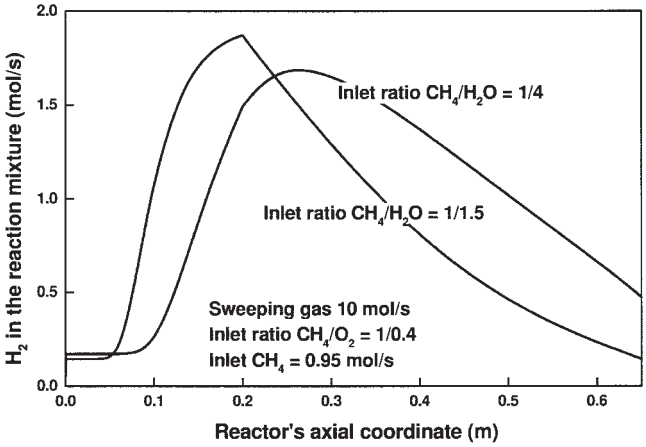

Figure 17. H_2 molar rate in the gas mixture at different inlet ratios of CH_4/H_2O to the reactor.

The sweeping gas flows at 10 mol/s in a counter-current mode.

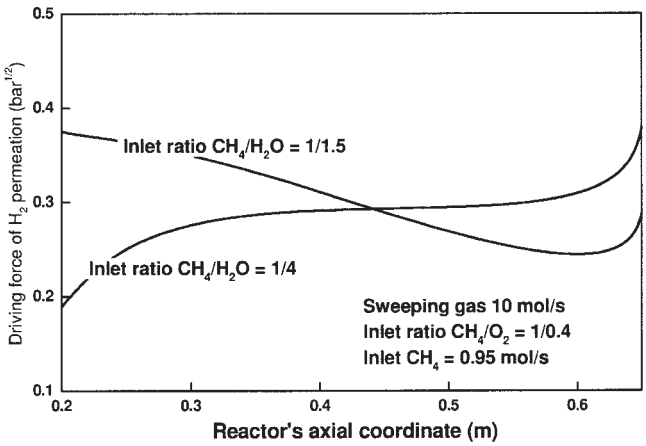

Figure 18. The driving force of H_2 permeation at different inlet CH_4/H_2O ratios to the reactor.

The sweeping gas flows at 10 mol/s in a counter-current mode.

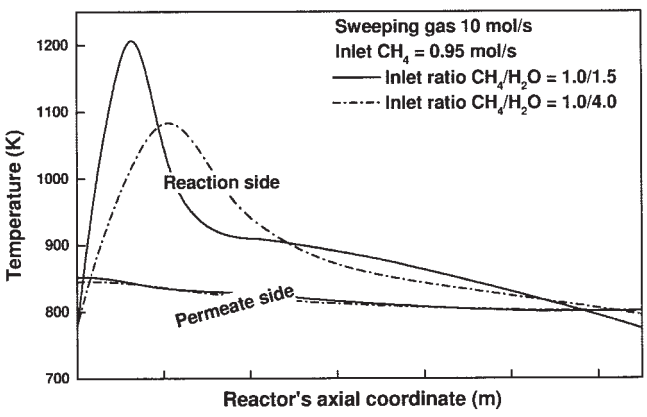

Figure 19. The axial temperature profiles at different inlet ratios of CH_4/H_2O to the reactor.

The sweeping gas flows at 10 mol/s in a counter-current mode. Inlet ratio of CH_4/O_2 = 1.0/0.4.

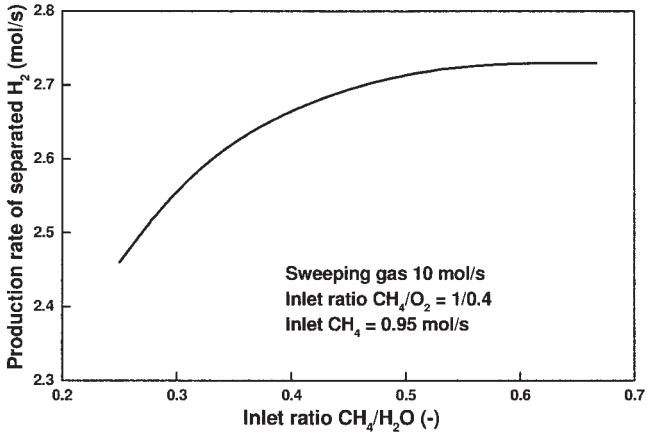

Figure 20. The production rate of separated H_2 vs. the inlet ratio of CH_4/H_2O to the reactor.

The sweeping gas flows at 10 mol/s in a counter-current mode.

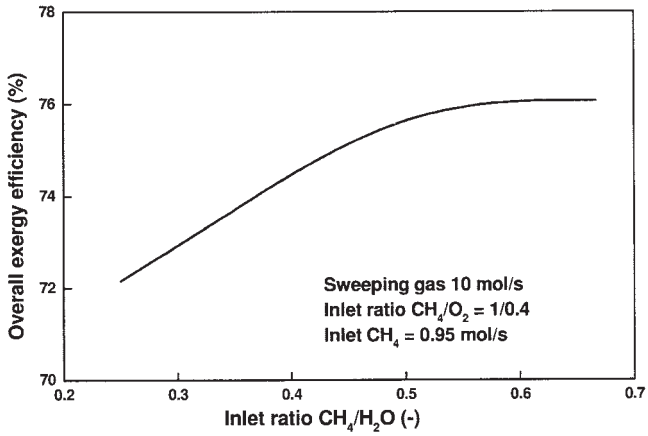

Figure 21. The overall exergy efficiency of the integrated process vs. the inlet ratio of CH_4/H_2O to the reactor.

The sweeping gas flows at 10 mol/s in a counter-current mode.

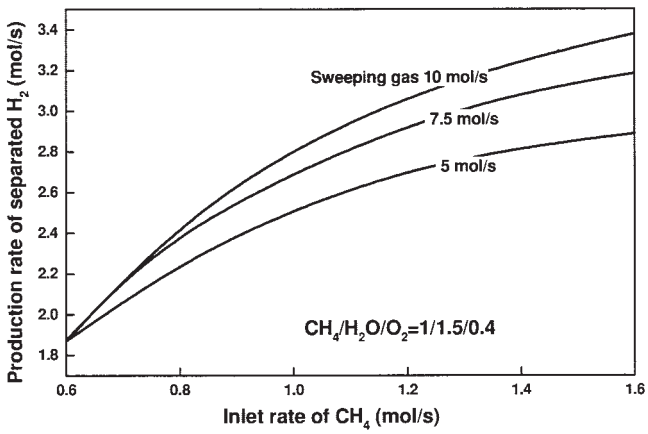

Figure 22. The production rate of separated H_2 at different inlet rates of sweeping gas as a function of inlet rate of CH_4 to the reactor.

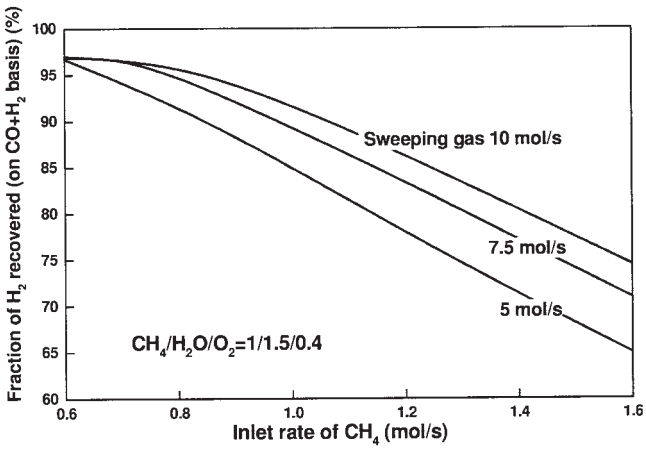

Figure 23. The fraction of H_2 recovered at different inlet rates of sweeping gas as a function of the inlet rate of CH_4 to the reactor.

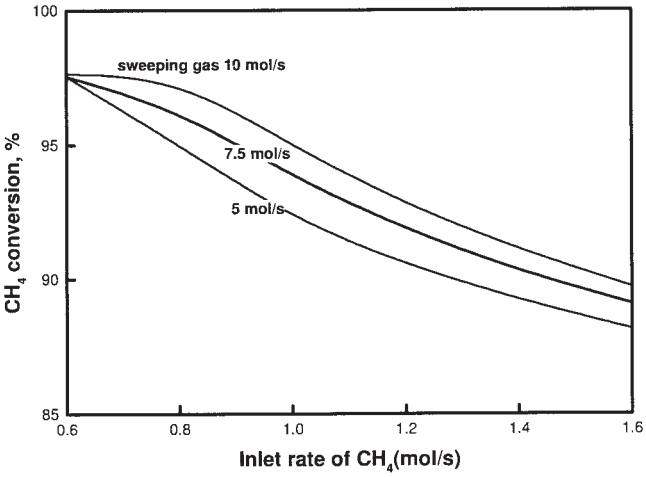

Figure 24. The methane conversion at different rates of sweeping gas as a function of the inlet rate of CH_4 to the reactor.

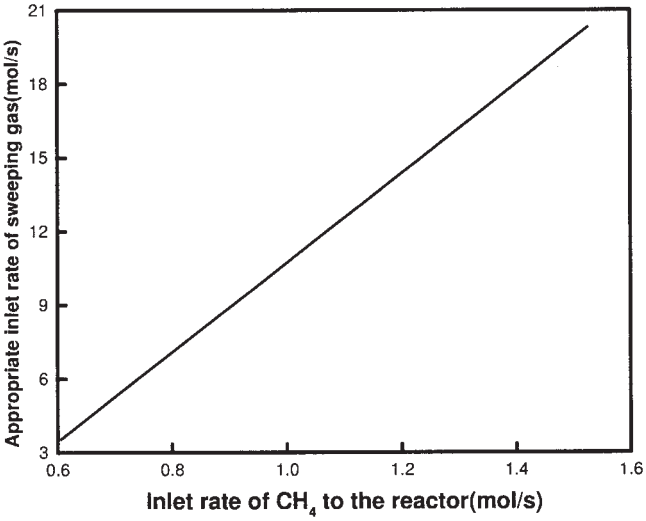

Figure 25. The appropriate inlet rate of sweeping gas as a function of the inlet rate of CH_4 to the reactor.

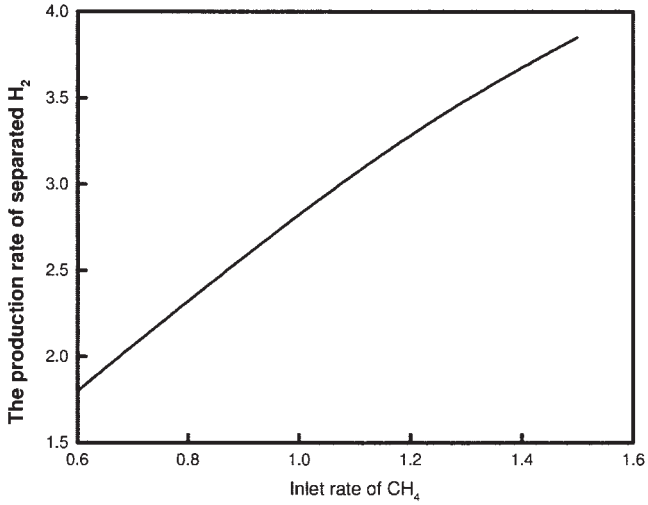

Figure 26. The production rate of H_2 separated corresponding to the appropriate inlet rate of sweeping gas as a function of the inlet rate of CH_4 to the reactor.

found, at which the sweeping gas is just sufficient for the H_2 membrane to separate the hydrogen maximally.

Acknowledgement

This work was supported by The National Science Foundation of China (Grant No. 20325622, 20576013, 90210032, 50576001).

Notation

a_{H_2} = cross section area of reactor, m^2
H_2 = membrane area per unit reactor length, m^2/m
a_v = area of particle per unit mass of catalyst, m^2/kg
$C_{p,i}$ = heat capacity of species i [J/(mol k)]
$C_{p,j}$ = heat capacity of species j [J/(mol k)]
$D_{e,j}$ = effective diffusion coefficient of species i in catalyst pellet [m^2/s]
E_A = apparent activation energy of H_2 membrane, J/mol
$E_{a,k}$ = activation energy of reaction k, J/mol
Ex = exergy flow rate, J/s
F_i = molar flow rate of i, mol/s
$F_{extra}CH_4$ = molar flow rate of extra methane to the catalytic burner, mol/s
F_l = molar flow rate of combustible component l in the rejected gas, mol/s
G_{H_2} = molar flow rate of H_2 in the non-reaction side, mol/s
G_j = molar flow rate of component j in the non-reaction side, mol/s
K_{eq} = equilibrium constant
K_i = adsorption constant of species i
K_i^0 = pre-exponential factor for adsorption parameters
k_e = thermal conductivity of catalyst bed, J/(m s K)
k_k = reaction rate constant of reaction k
K_k^0 = pre-exponential factor for reaction rate, mol/(kg_{cal} s)
k_m = averaged thermal conductivity of the membranes, J/(m s K)
k_{sp} = thermal conductivity of membrane support layer, J/(m s K)
L = reactor length, m
N_{H_2} = H_2 permeation rate through the H_2 membrane, mol/(m^2 s)
$N_i^{H_2}$ = component i permeation rate through the H_2 membrane, mol/(m^2 s)
N_R = number of reactions
n_{tube} = number of membrane tubes
P_m = pre-exponential factor of the H_2 membrane, mol m/(s m^2 $bar^{0.5}$)
P_0 = pressure of the environment, 101.325kPa
$P_{s,i}$ = partial pressure of species i in catalyst particle, bar
P_i = partial pressure of species i in the gas phase, bar

$p_{H_2}^{high}$ = partial pressure of H_2 in the reaction side, bar
$p_{H_2}^{low}$ = partial pressure of H_2 in the non-reaction side, bar
P_{in} = inlet pressure of the H_2-membrane ATR reactor, bar
q = the heat flux between the reaction side and the non-reaction side, J/(s m)
R = gas constant, J/(mol K)
R_k = rate of reaction k in the main stream of the H_2-membrane ATR reactor, calculated with p_i, mol/(kg_{cat} s)
r_s = equivalent radius of the catalyst particle, m
$R_{s,k}$ = rate of reaction k inside the catalyst particle, calculated with $P_{s,i}$, mol/(kg_{cat} s)
r_1 = tube inside radius, m
r_2 = tube outside radius, m
r_3 = inner radius of the shell, m
T = absolute temperature, K
T_{fg} = temperature of rejected gas, K
$\bar{T}$ = average temperature of the membranes, K
T_0 = temperature of the environment, 298.15K
W_{cp} = work used for compression, J/s
x_i = molar fraction of species i
z = axial coordinate of the reactors, m

Greek letters

ϵ = void fraction of packing
δ_{H_2} = the thickness of the membrane layer, m
δ_{sp} = the thickness of the support layer, m
η_{cp} = the exergy efficiency of the compressor
η_{Ex} = overall exergy efficiency
η_k = effectiveness factor of reaction k
v_{ik} = stoichiometric coefficient of component i of reaction k
ρ_s = density of catalyst, kg/m^3
ζ = dimensionless pellet coordinate
$\Delta H_{ads,i}$ = standard adsorption enthalpy of component i, kJ/mol
ΔH_{H_2} = the heat transferred by permeating H_2 from the reaction side to the non-reaction side, J/mol
$\Delta H_{heating}$ = the heat required for heating the reactants, J/s
ΔH_k = the heat of reaction k, J/mol
ΔH_l^{com} = the combustion heat of component l, J/mol
$\Delta H|_{T_{ts}}^{T_0}$ = the heat of rejected gas from T_{fg} to T_0, J/s

Literature Cited

1. Froment GF. Production of synthesis gas by steam- and CO2-reforming of natural gas. *J Molecular Catalysis A Chemical.* 2000;163:147-156.
2. Chen Z, Prasad P, Yan Y, Elnashaie S. Simulation for steam reforming of natural gas with oxygen input in a novel membrane reformer. *Fuel Proc Technol*. 2003;83:235-252.
3. Freni S, Calogero G, Cavallaro S. Hydrogen production from methane through catalytic partial oxidation reaction. *J Power Sources.* 2000; 87:28-38.
4. Hagh BF. Optimization of autothermal reactor for maximum hydrogen production. *Int J Hydrogen Energy.* 2003;28:1369-1377.
5. De Smet CRH, de Croon MHJM, Berger RJ, Marin GB, Schouten JC. Design of adiabatic fixed-bed reactors for the partial oxidation of methane to synthesis gas. Application to production of methanol and hydrogen-for-fuel-cells. *Chem Eng Sci.* 2001;56:4849-4861.
6. Amphlett JC, Mann RF, Peppley BA. On board hydrogen purification for steam reformation/PEM fuel cell vehicle power plants. *Int J Hydrogen Energy.* 1996;21(8):673-678.
7. Avcl AK, Trimm DL, Önsan ZI. Quantitative investigation of catalytic natural gas conversion for hydrogen fuel cell applications. *Chem Eng J*. 2002;4027:1-11.
8. Golunski S. Hotspot™ fuel processor. *Platinum Metals Review.* 1998; 42(1):2-7.
9. Chen Z, Yan Y, Said Elnashaie SEH. Novel circulating fast fluidised-bed membrane reformer for efficient production of hydrogen from steam reforming of methane. *Chem Eng Sci.* 2003;58:4335-4349.
10. Basile A, Paturzo L, Lagana F. The partial oxidation of methane to syngas in a palladium membrane reactor: simulation and experimental studies. *Catalysis Today.* 2001;67:65-75.
11. Grace J, Adris AM, Lim J. Production of pure hydrogen by the fluidized bed membrane reactor process. 14th World Hydrogen Energy Conference, Montreal, Canada, June 9-13, 2002.
12. Ostrowski T, Giroir-Fendler A, Mirdatos C, Mleczko L. Comparative study of the catalytic partial oxidation of methane to synthesis gas in fixed-bed and fluidised-bed membrane reactors. *Catalysis Today.* 1998;40:181-190.
13. Trimm D, Lam CW. The combustion of methane on platinum-alumina fibre catalysts—I. *Chem Eng Sci.* 1980;35:1405-1413.
14. Xu J, Froment GF. Methane steam reforming, methanation and water gas shift: I. Intrinsic kinetics. *AIChE J.* 1989;35(1):88-96.
15. Xu J, Froment GF. Methane steam reforming: II. Diffusional limitations and reactor simulation. *AIChE J.* 1989;35(1):97-103.
16. Moore WJ. *Physical Chemistry*. Englewood Cliffs, NJ: Prentice-Hall International; 1972.
17. Smith JM, Van Ness HC, Abbott MM. *Introduction to Chemical Engineering Thermodynamics* (5th ed.). New York: McGraw-Hill; 1996.
18. Welty JR, Wilson RE, Wicks CE. Fundamentals of Momentum, Heat and Mass Transfer (2nd ed.). New York: Wiley; 1976.
19. Soomro M, Hughes R. The thermal conductivity of porous catalyst pellets. *Canadian J Chem Eng.* 1979;57:24-28.
20. Schack A. *Industrial Heat Transfer*. New York: Wiley; 1965.
21. Szargut J, Morris DR, Steward FR. *Exergy Analysis of Thermal, Chemical and Metallurgical Processes*. New York: Hemisphere Publishing Corporation; 1998.
22. Kjelstrup S, De Swaan Arons J. Denbigh revisited: reducing lost work in chemical processes. *Chem Eng Sci.* 1995;50:1551-1560.
23. Rosen MA, Scott DS. Entropy production and exergy destruction: Part II—Illustrative technologies. *Int J Hydrogen Energy.* 2003;28:1315-1323.

Manuscript received Oct. 21, 2005, and revision received Jan. 8, 2006.